Sciencexpress Research Article

Mapping the Antigenic and Genetic Evolution of Influenza Virus

Derek J. Smith,[1,2*†] Alan S. Lapedes,[3*] Jan C. de Jong,[2] Theo M. Bestebroer,[2] Guus F. Rimmelzwaan,[2] Albert D. M. E. Osterhaus,[2] Ron A. M. Fouchier[2*]

[1]Department of Zoology, University of Cambridge, Downing Street, Cambridge CB2 3EJ, UK. [2]National Influenza Center and Department of Virology, Erasmus Medical Center, Dr. Molewaterplein 50, 3015GE Rotterdam, Netherlands. [3]Theoretical division, T-13, MS B213, Los Alamos National Laboratory, Los Alamos, NM 87545, USA.

*These authors contributed equally to this work.
[†]To whom correspondence should be addressed. E-mail: dsmith@zoo.cam.ac.uk

The antigenic evolution of influenza A (H3N2) virus was quantified and visualized from its introduction into humans in 1968 through to 2003. Although there was remarkable correspondence between antigenic and genetic evolution, significant differences were observed: antigenic evolution was more punctuated than genetic evolution, and genetic change sometimes had a disproportionately large antigenic effect. The method readily allows monitoring of antigenic differences among vaccine and circulating strains, and thus estimation of the effects of vaccination. Further, this approach offers a route to predicting the relative success of emerging strains, which could be achieved by quantifying the combined effects of population level immune escape and viral fitness on strain evolution.

Much of the burden of infectious disease today is caused by antigenically variable pathogens that can escape from immunity induced by prior infection or vaccination. The degree to which immunity induced by one strain is effective against another is mostly dependent on the antigenic difference between the strains; thus, the analysis of antigenic differences is critical for surveillance and vaccine strain selection. These differences are measured in the laboratory in various binding assays (*1–3*). Such assays give an approximation of antigenic differences, but are generally considered unsuitable for quantitative analyses. We present a method, based on the fundamental ideas described by Lapedes and Farber (*4*), that enabled a reliable quantitative interpretation of binding assay data, increased the resolution at which antigenic differences can be determined, and facilitated visualization and interpretation of antigenic data. We used this method to study quantitatively the antigenic evolution of influenza A(H3N2) virus, revealing both similarities to, and important differences from, its genetic evolution.

Influenza viruses are classic examples of antigenically variable pathogens and have a seemingly endless capacity to evade the immune response. Influenza epidemics in humans cause an estimated 500,000 deaths worldwide per year (*5*). Antibodies against the viral surface glycoprotein hemagglutinin (HA) provide protective immunity to influenza virus infection and this protein is therefore the primary component of influenza vaccines. However, the antigenic structure of HA has changed significantly over time, a process known as antigenic drift (*6*), and in most years the influenza vaccine has to be updated to ensure sufficient efficacy against newly emerging variants (*7*, *8*). The World Health Organization coordinates a global influenza surveillance network, currently consisting of 112 national influenza centers and 4 collaborating centers for reference and research. This network routinely characterizes the antigenic properties of influenza viruses using a hemagglutination inhibition (HI) assay (*1*). The HI assay is a binding assay based on the ability of influenza viruses to agglutinate red blood cells and the ability of animal antisera raised against the same or related strains to block this agglutination (*9*). Additional surveillance information is provided by sequencing the immunogenic HA1 domain of the HA gene for a subset of these strains. The combined antigenic, epidemiological, and genetic data are used to select strains for use in the vaccine.

Retrospective quantitative analyses of the genetic data have revealed important insights into the evolution of influenza viruses (*10–13*). However, the antigenic data are largely unexplored quantitatively due to difficulties in interpretation, even though antigenicity is a primary criterion for vaccine strain selection and is thought to be the main driving force of influenza virus evolution. When antigenic data have been analyzed quantitatively, it has usually been with the methods of, or methods equivalent to, numerical taxonomy (*14–16*). These methods have provided insights (*15–19*); however, they sometimes give inconsistent results, do not properly interpret thresholded data, and approximate antigenic distances between strains in an indirect way

[discussed by (*4*, *16*, *18*)]. Lapedes and Farber (*4*) solved these problems with a geometric interpretation of binding assay data, in which each antigen and antiserum is assigned a point in an "antigenic map" [based on the theoretical concept of "shape space" (*20–23*)], such that the distance between an antigen and antiserum in the map directly corresponds to the HI measurement. Lapedes and Farber used ordinal multidimensional scaling (MDS) (*24*) to position the antigens and antisera in the map.

The method used in this manuscript is based on the fundamental ideas described by Lapedes and Farber (*4*), and in particular takes advantage of their observation that antigenic distance is linearly related to the logarithm of the HI measurement. Exploiting this observation allowed us to create a new method that is parametric, yet which still handles HI measurements that are beyond the sensitivity of the HI assay (*9*). We use a modification of metric MDS (*25*) to position the antigens and antisera in the map (*9*). This new approach offers computational advantages over the ordinal approach, including reduced running time and fewer local minima, making it tractable to run on datasets the size of the one used in this manuscript, and on larger datasets.

Antigenic map of human influenza A (H3N2) virus. We applied this method to mapping the antigenic evolution of human influenza A(H3N2) viruses, which became widespread in humans during the 1968 Hong Kong influenza pandemic and have been a major cause of influenza epidemics ever since. Antigenic data from 35 years of influenza surveillance between 1968 and 2003 were combined into a single dataset. We sequenced the HA1 domain of a subset of these virus isolates (*26*, *27*) and restricted the antigenic analysis to these sequenced isolates to facilitate a direct comparison of antigenic and genetic evolution. The resulting antigenic dataset consisted of a table of 79 post-infection ferret antisera by 273 viral isolates, with 4,215 individual HI measurements as entries in the table. Ninety-four of the isolates were from epidemics in The Netherlands and 179 were from elsewhere in the world.

We constructed an antigenic map from this dataset to determine the antigenic evolution of influenza A(H3N2) virus from 1968 to 2003 (Fig. 1). Since antigen-antiserum distances in the map correspond to HI values, it was possible to predict HI values that were missing in the original dataset, and subsequently measure those values using the HI assay, to determine the resolution of the map. We predicted and then measured 481 such HI values with an average absolute prediction error of 0.83 (SD 0.67) units (each unit of antigenic distance corresponds to a 2-fold dilution of the antiserum in the HI assay). The accuracy of these predictions indicate that the map has resolution higher than that previously considered available from HI data, and higher than the resolution of the assay. The resolution of the map can be greater than the resolution of the assay because the location of a point in the map is fixed by measurements to multiple other points, thereby averaging out errors (*9*).

The map reveals high-level features of the antigenic evolution of influenza A(H3N2) virus. The strains tend to group in clusters rather than form a continuous antigenic lineage, and the order of clusters in the map is mostly chronological; from the original Hong Kong 1968 (HK68) cluster, to the most recent Fujian 2002 (FU02) cluster. The antigenic distance from the HK68 cluster, through consecutive cluster centers, to the FU02 cluster is 44.6 units, and the average antigenic distance between the centers of consecutive clusters is 4.5 (SD 1.3) units. The influenza vaccine is updated between influenza seasons when there is an antigenic difference of at least 2 units between the vaccine strain and the strains expected to circulate in the next season; thus not unexpectedly, we find at least one vaccine strain in each cluster.

The ability to define antigenic clusters allows us to identify the amino acid (aa) substitutions that characterize the difference between clusters (Table 1, fig. S1). Some of these "cluster-difference" substitutions (*9*) will contribute to the antigenic difference between clusters, some might be compensatory mutations to retain function, and others might be hitchhikers carried along by chance. Of the 67 cluster-difference aa substitutions, 63 were in antigenic sites (*28*), 8 were in the receptor-binding site (*29*), and 21 were in codons previously identified as positively-selected in an independent genetic dataset covering 1985 to 1997 (*10*). We see two patterns with respect to these positively-selected codons: for the cluster transitions which happened during the period from 1985 to 1997—the period of the sample used to calculate the positively-selected codons—most (10 of 12) of the cluster-difference substitutions were in positively-selected codons; whereas outside of this timeframe most (44 of 55, or 16 of 20 if the underrepresented TX77 and FU02 clusters are excluded) were not in positively-selected codons. A possible explanation for this difference is that cluster-difference substitutions are positively selected, but that the positively-selected codons have changed over time, resulting in some pre-1985 positively-selected codons not being previously identified, possibly because they were underrepresented in the dataset used by (*10*). Other possible explanations are that not all cluster-difference substitutions are positively selected, or that they cannot be detected as such with methods that use only genetic information.

Comparison of antigenic and genetic evolution. To further investigate the genetic basis of the antigenic cluster structure, we generated a maximum likelihood (ML) phylogenetic tree and a "genetic map" of the HA1 sequences of strains used in the antigenic analysis, and color-coded both according to the clusters identified in the antigenic map of

Fig. 1 (Fig. 2). The genetic map facilitates a side-by-side comparison with the antigenic map, and is a visualization of the aa distance matrix calculated from the alignment of HA1 sequences (*9*). Previous comparisons of the antigenic and genetic evolution have revealed important insights (*30, 31*); however, a quantitative comparison has not been possible until now because of the previously low resolution in the antigenic data.

We find a remarkable overall correspondence between the relative positions of clusters in the genetic and antigenic maps (Figs 2B and C, respectively). The correlation between antigenic distance and the number of aa substitutions between strains was 0.81, and on average 2.9 aa substitutions resulted in one unit change in antigenic distance. The rate of antigenic evolution per aa substitution was slower within clusters (on average 3.1 (SD 0.06) aa substitutions for each unit of antigenic change) than between clusters (on average 2.1 (SD 0.17) aa substitutions for each unit of antigenic change).

There is also a correspondence between the phylogenetic tree and antigenic map, with closely related nucleotide sequences generally belonging to the same antigenic cluster (Figs 2A and C). The correlation between antigenic distance and ML phylogenetic tree distance between strains was 0.78, and on average an ML distance of 0.0085 corresponded to a one unit change in antigenic distance.

Although antigenic clusters are mostly contiguous when shown on the phylogenetic tree and genetic map (Fig. 2, A and B), it is not possible to reliably determine antigenic clusters from genetic data alone. From the tree it is rarely obvious if a branch or lineage belongs to the same or a different antigenic cluster as its neighbors, and from the genetic map it is not always possible to determine where one antigenic cluster ends and another begins. The most striking example is the distance between the SI87 and BE89 clusters, which are genetically closely related but antigenically distinct. The difficulties with an antigenic interpretation of genetic data include the variation in the antigenic effect of aa substitutions due to either the particular aa substitution, the location of the substitution, or the interaction of multiple substitutions.

Surprisingly, a single aa substitution, N145K, is the only cluster-difference substitution between the SI87 and BE89, and between the Beijing 1992 (BE92) and WU95 clusters. This is surprising because other cluster transitions are characterized by multiple cluster-difference substitutions, and because on average a single aa substitution causes only 0.37 units of antigenic change. Three pieces of evidence however indicate that N145K has a large antigenic effect, and thus alone can be responsible for a cluster transition. First, there are 12 pairs of strains in the dataset that only differ by N145K, and the average antigenic distance between these pairs in the antigenic map is 4.0 units (SD 1.1). In contrast, other aa substitutions at the same position (I145S, N145S), and the same substitution at a different position (N92K), each resulted in less than 1 unit of antigenic change. Second, we took a strain from the BE92 cluster and performed experimental site-directed mutagenesis of position 145 from N to K and this resulted in 2.6 units of antigenic difference. Third, there were nine strains in the genetic map for which the genetic cluster did not correspond with the antigenic cluster, and for which N145K was responsible. These nine strains were interdigitated between the BE92 and WU95 clusters: five strains from the BE92 antigenic cluster were genetically WU95-like but lacked the N145K substitution (seen as pink triangles in the green WU95 genetic cluster, Fig. 3); and vice-versa, four strains from the WU95 antigenic cluster were genetically BE92-like but had the N145K substitution (shown as green circles in the pink BE92 genetic cluster, Fig. 3). To exclude the possibility of laboratory errors, we resequenced and regenerated the HI data for seven of these interdigitated strains and obtained the same results. These three pieces of evidence indicate that a single aa substitution, in this case N145K, can cause sufficient antigenic change to be responsible for a cluster transition. Thus, although there is a remarkable correspondence between the genetic and antigenic evolution, there are exceptions that have epidemiological significance of sufficient magnitude that they require an update of the vaccine strain.

Gradual genetic evolution, but punctuated antigenic evolution. A season-by-season analysis of the clusters in the antigenic map shows that in some seasons strains were isolated from more than one antigenic cluster (Fig. 4A). On average clusters remained dominant for 3.3 years (SD $\pm$ 1.9), with two clusters being dominant for only one season, and one for eight seasons. In this dataset we see strains appear in a cluster up to two years before, and two years after, the period in which that cluster is the dominant cluster.

The corresponding season-by-season analysis of ML tree distances (Fig. 4B) shows the rate of genetic change to be relatively continuous compared to the antigenic evolution (Fig. 4A), which is more punctuated. Since this may in part be due to silent nucleotide substitutions, we repeated the analysis using the number of aa substitutions between strains instead of the ML tree distance (Fig. 4C) and found gaps between some clusters, but still a gradual accumulation of mutations which is not reflected in the corresponding antigenic figure, suggesting that some of these aa substitutions have little antigenic effect or an effect spreading the cluster sideways in relation to the distance from A/Bilthoven/16190/68 antigen.

The average rates of evolution are given by the slope of the best linear fit to the data in Fig. 4, A, B, and C. The average rate of antigenic drift calculated this way was 1.2 units per year, the average rate of aa substitutions was 3.6 per

year, and the average rate of change in ML distance was 0.0060 per year. Sometimes the rate of antigenic evolution was faster than genetic evolution, and sometimes vice-versa, as shown by the deviations from the linear regression line in Fig. 4D, again indicating a remarkable correspondence, with significant exceptions.

The observed pattern of clustered antigenic drift with similar antigenic distances between consecutive cluster centroids, is similar to that observed by Gog and Grenfell in a theoretical model in which strain dynamics were governed by a combination of epidemiology and cross-reactive immunity based on antigenic distance (*32*). This similarity is phenotypic evidence that escape from immunity in the human population plays a major role in determining influenza strain dynamics. Furthermore, there is a selective advantage for clusters that move away linearly from previous clusters as they most effectively escape existing population-level immunity, and this is a plausible explanation for the somewhat linear antigenic evolution in regions of the antigenic map (Fig. 1). The observed deviations from a linear path, as well as the rate of the antigenic evolution, might be determined by tradeoffs between intrinsic viral fitness and extrinsic fitness determined by population-level immunity, possibly in concert with stochastic seeding processes (*33*), short-lived broad immunity (*13*), and the phylodynamics of the virus (*34*).

Genetic analyses of Darwinian selection on influenza HA have focused on the gene-level, with more recent refinements to the codon-level (*10*). The quantification of antigenic data described here, which allows the estimation of the antigenic effect of individual aa substitutions, provides the opportunity for analyses which integrate selection at the phenotypic level with genetic change at the level of individual aa substitutions.

In summary, we have presented a quantification and visualization of the antigenic evolution of influenza A (H3N2) virus from 1968 to 2003, and have tested the accuracy of the method using blind prediction. We show that antigenic evolution is clustered and mostly two-dimensional, a higher rate of antigenic evolution between clusters than within clusters, a remarkable correspondence between antigenic and genetic evolution, but with important exceptions of epidemiological significance, and a punctuated antigenic evolution compared to a more continuous genetic evolution. The data used for this study were collected as part of routine influenza surveillance, and although there are significant biases in such data, these biases do not have a significant effect on the results (*9*). This is the most detailed characterization of a real antigenic shape space to date.

From a public health perspective, these methods increase the value of surveillance data, and facilitate vaccine strain selection, by allowing: a finer-grain interpretation of antigenic data, a way to interpret complex data in a simple visual format, and a further integration of antigenic and genetic data. In addition, antigenic maps, in conjunction with strain prevalence data, could be used to quantify the extent to which emerging strains escape immunity in the human population. This would allow the immune-escape component of viral fitness to be compared among multiple cocirculating strains, and if immune-escape is a dominant aspect of total fitness, be a predictor of which strains would be more likely to seed a new epidemic. It might also be possible to increase the efficacy of repeated vaccination by accounting quantitatively for the antigenic distances among vaccine strains (*23*).

We have used human influenza A(H3N2) virus to develop and validate analyses of antigenic properties from binding assay data. We have applied the same methods to the characterization of human H1N1, swine H3N2, and equine H3N8 influenza A viruses, and human influenza B virus. There are no assumptions that limit the use of these methods to influenza virus and the HI assay, and we have also applied the methods to the recognition of epitopes by cytotoxic T lymphocytes. We expect these methods will apply to other binding assays such as virus neutralization, compliment fixation, and ELISA (*35*), and that they will be useful for a wide variety of antigenically variable pathogens including human immunodeficiency virus and hepatitis C virus. In general, these methods facilitate the analyses of phenotypes similarly to the way phylogenetic algorithms facilitate analyses of genotypes. Such quantitative analyses have potentially wide-ranging implications for strain surveillance, vaccine strain selection, and for applied and basic research involving antigenically variable pathogens.

References and Notes

1. G. K. Hirst, *J. Exp. Med.* **78**, 407 (1943).
2. D. D. Richman, T. Wrin, S. J. Little, C. J. Petropoulos, *Proc. Natl. Acad. Sci. U.S.A.* **100**, 4144 (2003).
3. D. H. O'Connor *et al.*, *Nature Med.* **8**, 493 (2002).
4. A. Lapedes, R. Farber, *J. Theor. Biol.* **212**, 57 (2001).
5. K. Stohr, *Lancet Infect. Dis.* **2**, 517 (2002).
6. A. W. Hampson, in *Influenza*, C. W. Potter, Ed. (Elsevier, London, 2002), pp. 49–85.
7. J. E. Salk, P. C. Suriano, *Am. J. Publ. Health* **39**, 345 (1949).
8. E. D. Kilbourne *et al.*, *Proc. Natl. Acad. Sci. U.S.A.* **99**, 10748 (2002).
9. Materials and methods are available as supporting material on *Science* Online.
10. R. M. Bush, W. M. Fitch, C. A. Bender, N. J. Cox, *Mol. Biol. Evol.* **16**, 1457 (1999).
11. R. M. Bush, C. A. Bender, K. Subbarao, N. J. Cox, W. M. Fitch, *Science* **286**, 1921 (1999).
12. J. B. Plotkin, J. Dushoff, S. A. Levin, *Proc. Natl. Acad. Sci. U.S.A.* **99**, 6263 (2002).

13. N. M. Ferguson, A. P. Galvani, R. M. Bush, *Nature* **422**, 428 (2003).
14. P. H. A. Sneath, Sokal, R. R., *Numerical Taxonomy* (Freeman, San Francisco, CA, 1973).
15. T. F. Weijers *et al.*, *J. Virol. Methods* **10**, 241 (1985).
16. D. J. Alexander *et al.*, *Avian Pathol.* **26**, 399 (1997).
17. P. A. Underwood, *J. Gen. Virol.***62 (Pt 1)**, 153 (1982).
18. A. Dekker, G. Wensvoort, C. Terpstra, *Vet. Microbiol.* **47**, 317 (1995).
19. J. M. Daly *et al.*, *J. Gen. Virol.***77** (Pt 4), 661 (1996).
20. A. S. Perelson, G. F. Oster, *J. Theor. Biol.* **81**, 645 (1979).
21. L. Edelstein, R. Rosen, *J. Theor. Biol.* **73**, 181 (1978).
22. D. J. Smith, S. Forrest, A. S. Perelson, in *Artificial Immune Systems and Their Applications* D. Dasgupta, Ed. (Springer Verlag, Berlin, 1998), pp. 105.
23. D. J. Smith, S. Forrest, D. H. Ackley, A. S. Perelson, *Proc. Natl. Acad. Sci. U.S.A.* **96**, 14001 (1999).
24. J. Kruskal, *Psychometrika* **29**, 115 (1964).
25. R. Shepherd, *Hum. Factors* **5**, 33 (1963).
26. Accession numbers.
27. C. A. Macken, H. Lu, J. Goodman, L. Boykin, in *Options for the Control of Influenza IV* A. D. M. E. Osterhaus, N. Cox, A. W. Hampson, Eds. (Elsevier Science B.V., Amsterdam, 2001), pp. 103.
28. D. C. Wiley, I. A. Wilson, J. J. Skehel, *Nature* **289**, 373 (1981).
29. I. A. Wilson, J. J. Skehel, D. C. Wiley, *Nature* **289**, 368 (1981).
30. G. W. Both, M. J. Sleigh, N. J. Cox, A. P. Kendal, *J. Virol.* **48**, 52 (1983).
31. A. J. Hay, V. Gregory, A. R. Douglas, Y. P. Lin, *Philos. Trans. R. Soc. London B. Biol. Sci.* **356**, 1861 (2001).
32. J. R. Gog, B. T. Grenfell, *Proc. Natl. Acad. Sci. U.S.A.* **99**, 17209 (2002).
33. J. R. Gog, G. F. Rimmelzwaan, A. D. Osterhaus, B. T. Grenfell, *Proc. Natl. Acad. Sci. U.S.A.* **100**, 11143 (2003).
34. B. T. Grenfell *et al.*, *Science* **303**, 327 (2004).
35. D. A. Lennette, in *Diagnostic Procedures for Viral, Ricketssial and Chlamydial Infections,* E. H. Lennette, D. A. Lennette, E. T. Lennette, Eds. (American Public Health Association, Washington, DC, 1995).
36. B. Korber *et al.*, *Science* **288**, 1789 (2000).
37. We thank Ruud van Beek, Walter Beyer, Tanmoy Bhattacharya, Robin Bush, Nancy Cox, Bryan Grenfell, Julia Gog, Howard Gutowitz, Alan Hay, Ron Hightower, Terry Jones, Akaysha Tang, the contributors to the WHO global influenza surveillance network and the maintainers of the Influenza Sequence Database (www.flu.lanl.gov). We acknowledge the support of the Santa Fe Institute and the Dutch National Institute of Public Health and the Environment (RIVM). DJS was supported by European Union grant QLRT-2001-01034. ASL was supported by the US Department of Energy under contract W-7405-ENG-36. RAMF is a fellow of the Royal Dutch Academy of Arts and Sciences.

Supporting Online Material

www.sciencemag.org/cgi/content/full/1097211/DC1
Materials and Methods
Figures S1 to S3
Table S1
References and Notes

26 February 2004; accepted 11 June 2004
Published online 24 June 2004; 10.1126/science.1097211
Include this information when citing this paper

Fig. 1. Antigenic map of influenza A(H3N2) virus from 1968 to 2003. The relative positions of strains (colored shapes) and antisera (uncolored open shapes) were adjusted such that the distances between strains and antisera in the map represent the corresponding HI measurements with the least error (*9*). The periphery of each shape denotes a 0.5 unit increase in the total error, thus size and shape represent a confidence area in the placement of the strain or antiserum. Strain color represents the antigenic cluster to which the strain belongs. Clusters were identified by a *k*-means clustering algorithm (*9*), and named after the first vaccine-strain in the cluster—two letters refer to the location of isolation (Hong Kong, England, Victoria, Texas, Bangkok, Sichuan, Beijing, Wuhan, Sydney, and Fujian) and two digits refer to year of isolation. The vertical and horizontal axes both represent antigenic distance, and because only the relative positions of antigens and antisera can be determined, the orientation of the map within these axes is free. The spacing between grid lines is one unit of antigenic distance—corresponding to a 2-fold dilution of antiserum in the HI assay. Two units correspond to 4-fold dilution, three units to 8-fold dilution, etc..

Fig. 2. Comparison of antigenic and genetic evolution of influenza A virus. (**A**) Phylogenetic tree of the HA1 sequences, color-coded based on antigenic clusters of Fig. 1. Multiple trees were built using a reversible site-dependent nucleotide maximum likelihood method (*36*). There was good consensus among trees, and the tree with maximum likelihood is shown. (**B**) Genetic map of the HA1 aa sequences, color-coded according to the antigenic clusters of Fig. 1. The vertical and horizontal axes represent genetic distance, in this case the number of aa substitutions between strains; the spacing between grid lines is 2.5 aa substitutions. The orientation of the map was chosen to match the orientation of the antigenic map in Fig. 1. (**C**) The same antigenic map of influenza A virus strains as shown in Fig. 1, except for a rigid-body rotation and translation of the pre-TX77 clusters (fig. S2) to match the genetic map, and that virus strains are represented by colored circles and antisera by

open squares. Arrows indicate the two cluster transitions for which the aa substitution N145K is the only cluster-difference substitution (Tab. 1, fig. S1).

Fig. 3. Detail of the genetic map (Fig. 2B) showing the BE92 and WU95 clusters and how a single aa substitution can determine the antigenic cluster. Pink and green symbols represent strains from the BE92 and WU95 antigenic clusters respectively. Ovals are drawn around the BE92 (circles) and WU95 (triangles) genetic clusters. Green symbols have a lysine (K) at position 145, whereas pink symbols have an asparagine (N) at 145. This single N145K substitution can cause an antigenic cluster change and warrant an update of the vaccine. Two pink triangles are coincident thus only four of the five can be seen. Grid and axes are the same as for Fig. 2B.

Fig. 4. Rates of antigenic and genetic evolution of influenza A virus. (**A**) Season-by-season analysis of antigenic evolution. Circle centers give the average antigenic distance to A/Bilthoven/16190/68 (BI/16190/68) antigen (*9*) for strains in each antigenic cluster and season, and are color-coded with the antigenic cluster colors of Fig. 1. The area of the circles represents the proportion of strains per season found in each antigenic cluster. Since sampling is biased toward outlier strains, these proportions do not reflect their epidemic impact. (**B**) Same as panel A but with ML-tree distances calculated from the phylogenetic tree (Fig. 2A). (**C**) Same as panel A but with aa substitution distances calculated from the genetic map (Fig. 2B). (**D**) Comparison of antigenic and genetic evolution. Points are color-coded according to antigenic cluster. The solid line connects the cluster centroids, the dashed line is the best linear fit to the data with a forced zero-intercept.

Table 1. Cluster-difference amino acid substitutions, and distances between antigenic clusters. Cluster-difference aa substitutions defined in (*9*), antibody binding sites defined by (*28*). ‡ Substitution at positively-selected codon (*10*); † at codon with rapid rate of aa replacement but not positively-selected (*11*); and * at codon in receptor binding site (*29*). The TX77 and FU02 clusters are represented by fewer strains than other clusters; thus, the number of cluster-difference substitutions into and out of these clusters might decrease with more strains in these clusters. Cluster transitions follow the chronological order of cluster dominance, which is occasionally different from the genetic lineage. Antigenic and genetic distances are between cluster centroids in the antigenic map (Fig. 1) and genetic map (Fig. 2B) respectively. The average standard error (SE) for the genetic distances between clusters was 0.9, for the antigenic distances between clusters was 0.3, and for the ratio was 0.3 (table S1).

Cluster transition	Genetic distance (aa changes)	Antigenic distance (units)	Genetic antigenic ratio	Cluster-difference substitutions					
				Site A	Site B	Site C	Site D	Site E	Other
HK68-EN72	12.1	3.4	3.6	T122N G144D	T155Y[*] N188D		R207K		
EN72-VI75	14.6	4.4	3.3	N137S[*†] S145N[‡]	L164Q Q189K S193D[‡]	N53D I278S	F174S R201K[‡] I213V I217V I230V		
VI75-TX77	14.8	3.4	4.4	S137Y[*†]	G158E[‡] Q164L D193N[‡]	K50R[†] D53N	S174F K201R[‡] V213I V230I	E82K M260I	
TX77-BA79	16.0	3.3	4.8	N133S[‡] P143S G146S	K156E[‡] T160K Q197R[‡]	N53D N54S	D172G[†] V217I V244L	I62K K82E	
BA79-SI87	11.9	4.9	2.4	G124D[‡]	Y155H[*] K189R				
SI87-BE89	6.9	4.6	1.5	N145K[‡]					
BE89-BE92	13.7	7.8	1.8	S133D[‡] K145N[‡]	E156K[‡] E190D[*‡]			T262N[‡]	
BE92-WU95	9.9	4.6	2.2	N145K[‡]					
WU95-SY97	16.0	4.7	3.4		K156Q[‡] E158K[‡] V196A[†]	N276K[†]		K62E	
SY97-FU02	16.0	3.5	4.5	A131T	H155T[*] Q156H[‡]	R50G[†]		H75Q E83K	L25I V202I W222R G225D[*]
Total	131.9	44.6							
Average	13.2	4.5	3.2						
SD	2.9	1.3	1.1						

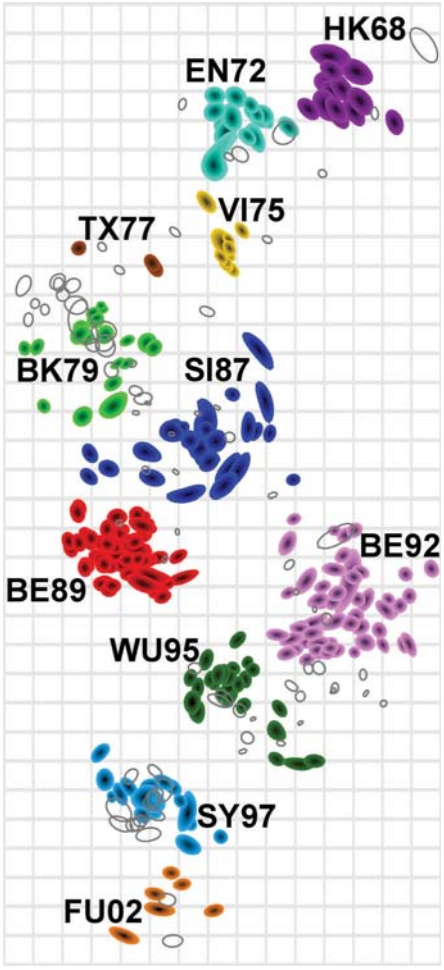
HK68
EN72
VI75
TX77
BK79
SI87
BE92
BE89
WU95
SY97
FU02

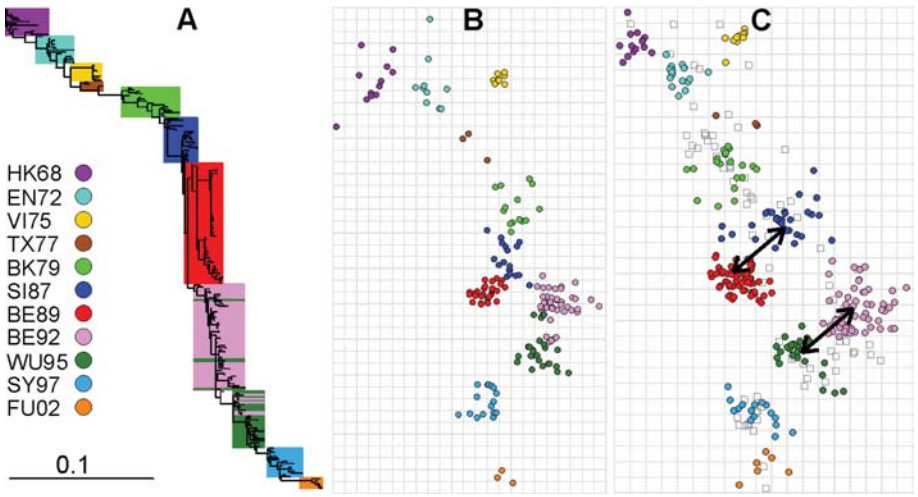
A
B
C
HK68
EN72
VI75
TX77
BK79
SI87
BE89
BE92
WU95
SY97
FU02
0.1

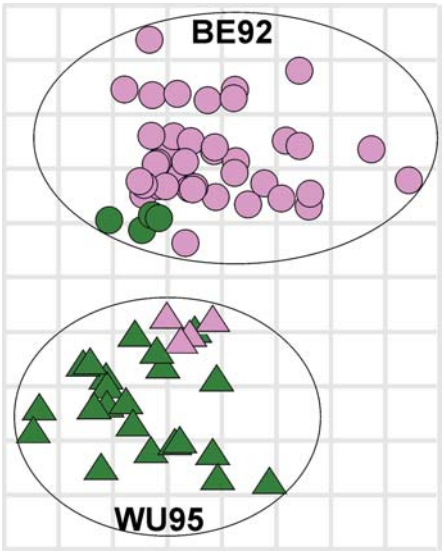
BE92
WU95

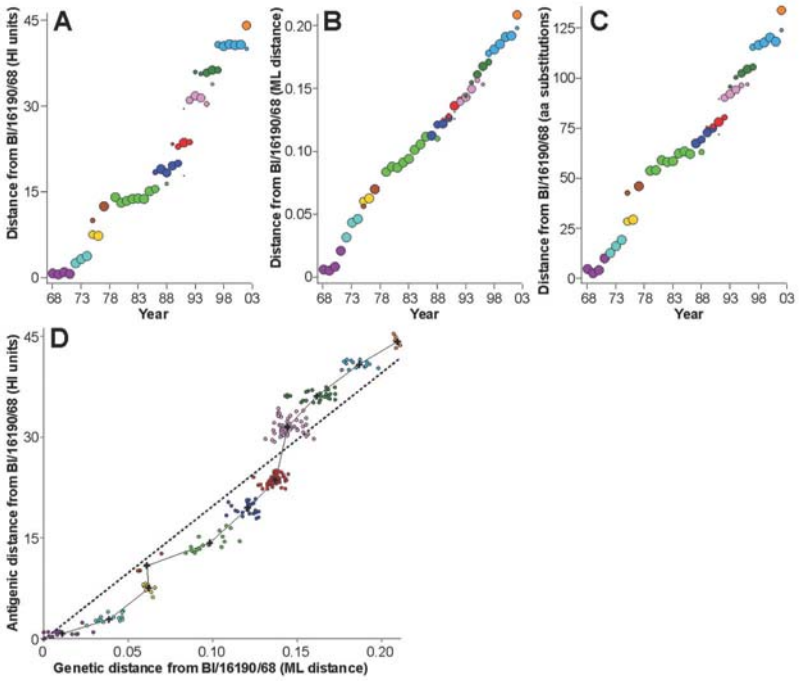
A
Distance from BI/16190/68 (HI units)
45
30
15
0
68 73 78 83 88 93 98 03
Year
B
Distance from BI/16190/68 (ML distance)
0.20
0.15
0.10
0.05
0
68 73 78 83 88 93 98 03
Year
C
Distance from BI/16190/68 (aa substitutions)
125
100
75
50
25
0
68 73 78 83 88 93 98 03
Year
D
Antigenic distance from BI/16190/68 (HI units)
45
30
15
0
0 0.05 0.10 0.15 0.20
Genetic distance from BI/16190/68 (ML distance)